Published in final edited form as:
*J Magn Reson Imaging*. 2014 July ; 40(1): 229–238. doi:10.1002/jmri.24345.

# Feasibility of 3-D MRI of Proximal Femur Microarchitecture at 3 T using 26 Receive Elements without and with Parallel Imaging

**Gregory Chang, M.D.**[1], **Cem Deniz, Ph.D.**[2], **Stephen Honig, M.D.**[3], **Chamith S. Rajapakse, Ph.D.**[4], **Kenneth Egol, M.D.**[4], **Ravinder R. Regatte, Ph.D.**[2], and **Ryan Brown, Ph.D.**[2]

[1]Department of Radiology, Center for Musculoskeletal Care, NYU Langone Medical Center, 333 E. 38th Street, 6th Floor, Room 610, New York, NY 10016, USA

[2]Department of Radiology, Center for Biomedical Imaging, NYU Langone Medical Center, 660 First Avenue, 4th Floor, New York, NY 10016, USA

[3]Osteoporosis Center, Hospital for Joint Diseases, NYU Langone Medical Center, 301 E. 17th Street, Suite 1101, New York, NY 10016, USA

[4]Laboratory for Structural NMR Imaging, Department of Radiology, Hospital of the University of Pennsylvania, 3400 Spruce Street, Philadelphia, PA 19104, USA

[5]Department of Orthopaedic Surgery, Hospital for Joint Diseases, NYU Langone Medical Center, 301 E. 17th Street, 14th Floor, New York, NY 10016, USA

## Abstract

**Purpose—**High-resolution imaging of deeper anatomy such as the hip is challenging due to low signal-to-noise ratio (SNR), necessitating long scan times. Multi-element coils can increase SNR and reduce scan time through parallel imaging (PI). We assessed the feasibility of using a 26-element receive coil setup to perform 3 T MRI of proximal femur microarchitecture without and with PI.

**Materials and Methods—**This study had institutional review board approval. We scanned thirteen subjects on a 3 T scanner using 26 receive-elements and a 3-D FLASH sequence without and with PI (acceleration factors (AF) 2, 3, 4). We assessed SNR, depiction of individual trabeculae, PI performance (1/g-factor), and image quality with PI (1=non-visualization to 5=excellent).

**Results—**SNR maps demonstrate higher SNR for the 26-element setup compared to a 12-element setup for hip MRI. Without PI, individual proximal femur trabeculae were well-depicted, including microarchitectural deterioration in osteoporotic subjects. With PI, 1/g values for the 26-element/12-element receive-setup were 0.71/0.45, 0.56/0.25, and 0.44/0.08 at AF2, AF3, and AF4, respectively. Image quality was: AF1, excellent (4.8±0.4); AF2, good (4.2±1.0); AF3, average (3.3±1.0); AF4, non-visualization (1.4±0.9).

**Conclusion—**A 26-element receive-setup permits 3 T MRI of proximal femur microarchitecture with good image quality up to PI AF2.

Corresponding Author: Gregory Chang, M.D. Tel: (646) 501-7290, Fax: (646) 501-7432, gregory.chang@nyumc.org.
All authors have no conflicts of interests. All authors have no financial disclosures.

**Keywords**

Bone microarchitecture; hip; femoral neck; fracture; MRI; osteoporosis

## Introduction

Osteoporosis is a "systemic skeletal disease characterized by low bone mass and microarchitectural deterioration of bone tissue with a consequent increase in bone fragility and susceptibility to fracture" [1]. The hip, or proximal femur, is the most devastating site of osteoporotic fracture. In the United States, approximately 70% ($12 billion) of the direct annual costs in fracture care are attributable to hip fractures [2]. In the first year following hip fracture, the mortality rate increases to 20% [3]. Although there is an association between hip fracture and low bone mineral density (BMD), low BMD explains only 28% of hip fractures [4].

Bone microarchitecture is an important contributor to bone strength, and landmark high-resolution magnetic resonance imaging (MRI) studies have provided strong evidence that its deterioration may explain differences in individuals' fracture risk [5,6]. However, in vivo 3-dimensional (3-D) imaging of bone microarchitecture in the proximal femur has been difficult to achieve via any imaging modality. For computed tomography (CT) scanning, the photon detector width for even the latest 320-row detector CT scanners is 0.5 mm [7]; this is insufficient to resolve trabeculae, which are less than 0.5 mm in dimension. CT also requires the administration of ionizing radiation. For high-resolution peripheral quantitative computed tomography (HRpQCT) scanning, image voxel sizes of 0.081 mm isotropic can be achieved [8–10]. However, HRpQCT scanners are not widely available and they have small scanner bores permitting imaging of only the wrist or ankle. Finally, for high-resolution MRI (0.137–0.234 mm in-plane, 0.4–1.5 mm slice thickness), bone microarchitecture in the distal radius and distal tibia has been extensively studied due to the higher SNR associated with peripheral extremities [5,6]. However, MRI of proximal femur microarchitecture has been attempted only once [11]. In this key 2005 article, Krug et al. used a 4-element radiofrequency array to image the hip at 1.5 T and 3 T. This important study was the first to establish the potential of MRI as a tool to evaluate proximal femur structure. The authors also concluded that because of SNR limitations, the ability to spatially resolve trabeculae remained an issue, mandating a 2-D textural analysis of images.

It is challenging to spatially resolve individual trabeculae in the proximal femur with MRI because SNR decreases as the distance between the radiofrequency coil and the anatomic structure of interest increases. For example, compared to the distal tibia or radius, which may be less than 2 cm from the skin surface, the proximal femur may be 5 to 8 cm from the skin surface (and radiofrequency coil). Over the last several years, the development of multi-element coils has provided a means to: 1) improve the sensitivity for MRI signal detection and obtain higher image SNR and 2) improve parallel imaging performance [12,13]. For example, a 32-element receive array has been shown to increase image SNR (permitting better visualization of microstructural brain anatomy) and to improve parallel imaging performance compared to an 8-element receive array [13]. The goal of this work was to

determine whether a new 26-element receive coil setup (compared to a 12-element receive coil setup) for 3 T hip MRI would: 1) provide SNR gains allowing visualization of individual trabeculae composing proximal femur microarchitecture to be possible, and 2) also provide enough SNR to allow imaging of proximal femur microarchitecture to be possible with parallel imaging.

## Materials and Methods

### Subject Recruitment

This study had institutional review board approval and we obtained written informed consent from all subjects. From the Osteoporosis Center at our hospital, we recruited 13 subjects (3 males, 10 females, mean age = 65.4 ± 10.3 years) with dual-energy x-ray absoprtiometry (DXA) results spanning osteopenia and osteoporosis (mean total hip BMD T-score = −2.1 ± 1.2) and no history of fragility fractures.

### Assessment of SNR and Parallel Imaging Performance

All MRI scanning with the novel 26-element coil setup was performed on a 128 channel 3 T MRI scanner (Siemens Skyra, Erlangen, Germany). The novel 26-element coil setup was composed of a commercial flexible 18-element array coil anteriorly (Siemens, three rows of six elements, each measuring 9 cm × 12 cm) and 8 elements from a commercial 32-element spine coil posteriorly (Siemens, Erlangen, Germany; two rows of 4 elements, each element measuring 12 cm × 13 cm). As a comparison, we also measured SNR using a 12-element coil setup, which was composed of a commercial flexible 6-element array coil anteriorly (Siemens, Erlangen, Germany; two rows of three elements, each element measuring 16 × 15 cm) and 6 elements from a commercial 24-element spine coil posteriorly (Siemens, Erlangen, Germany; two rows of 3 elements, each element measuring 17 cm × 13 cm). The MRI scanning for the 12-element coil setup was performed on a Siemens Trio 3 T MRI scanner due to coil compatibility. In brief, we obtained gradient echo images (TR/TE=200 ms/4.92ms, slice thickness=3 mm, matrix=256 × 256, field-of-view=220 mm) and saved raw k-space data. We obtained a noise reference measurement by recording data during the same sequence but without radiofrequency excitation. From the estimates of noise covariance and coil sensitivity, SNR maps were calculated in MatLab (MathWorks, Natick, Massachusetts, USA) using the method of Kellman et al [14,15]. To assess parallel imaging performance, we computed inverse geometry (1/g) factor maps in the coronal plane according to Eq. 23 from Pruessmann et al.[16].

### MRI of Bone Microarchitecture

We scanned the dominant hip of subjects using a 3-D fast low angle shot sequence (TR/TE=37 ms/4.92 ms, matrix=512 × 512, field-of-view=12 cm, slice thickness=1.5 mm, 60 coronal images, acquisition time = 29 minutes 31 seconds) without and with parallel imaging (generalized autocalibrating partially parallel acquisition (GRAPPA), 24 reference lines) at acceleration factors of two (acquisition time = 15 minutes 18 seconds), three (acquisition time = 10 minutes 30 seconds), and four (acquisition time = 8 minutes 6 seconds). Because MR images show trabeculae as hypointense and marrow as hyperintense, we also inverted the images (simple linear transformation) to obtain traditional contrast

where trabeculae are hyperintense and marrow are hypointense, which is more visually pleasing to referring clinicians.

A musculoskeletal radiologist (7 years experience in bone microarchitecture MRI methods) and an imaging scientist (8 years of experience in bone microarchitecture MRI methods and digital image analysis) independently evaluated the images for each subject at each acceleration factor on a five-point Likert scale to determine whether individual trabeculae could be visualized (1 = non-visualization, 2 = poor, 3 = average, 4 = good, 5 = excellent). The images were presented in a randomized order and the reviewers were blinded to the imaging parameters. For each subject, we obtained a mean image quality score at each acceleration factor. Finally, a student's t-test was performed to determine whether there were significant differences ($p < 0.05$) in mean image quality for all subjects at AF1 compared to AF2, AF2 compared to AF3, and AF3 compared to AF4.

## Results

First, we compared the SNR provided by the new 26-element coil setup and a 12-element coil setup used for hip MRI (Figure 1). The 26-element coil setup did provide higher SNR for imaging of the proximal femur compared to the 12-element coil. The SNR gains were approximately 4 to 5-fold in the greater trochanter, 3-fold in the intertrochanteric region, and 2-fold in the femoral neck (Figure 1b). Next, we evaluated parallel imaging performance using the 26-element receive coil setup and the 12-element coil setup. Figure 2 shows inverse g-factor maps for the 26-element coil setup compared to the 12-element coil setup. 1/g values measured in the femoral neck for the 26-element coil setup were 0.71, 0.56, and 0.44, at acceleration factors 2, 3, and 4, respectively. 1/g values measured in the femoral neck for the 12-element coil setup were 0.45, 0.25, and 0.08, at acceleration factors 2, 3, and 4, respectively. The higher 1/g values for the 26-element coil setup represents greater SNR retained for a given acceleration factor. Note that a 1/g value of unity indicates no SNR penalty due to parallel imaging reconstruction, while a value of zero indicates an infinite penalty.

We then assessed whether the higher SNR of the 26-element coil setup could be used to depict individual trabeculae composing proximal femur microarchitecture. We first tried this without parallel imaging, since this incurs an SNR penalty. Figure 3 shows representative MR images of the proximal femur obtained with the 26-element coil setup and the 12-element coil setup in the same subject. Individual trabeculae can be seen within the proximal femur using the 26-element coil setup, but they are harder to visualize with the 12-element coil setup. Figure 4 shows representative images obtained in five other subjects scanned with the 26-element coil setup. Because referring clinicians are habituated to looking at images with bone in white and marrow as dark, we also inverted the images (simple linear transformation) to demonstrate the images that could potentially be shown to referring clinicians (Figure 4). The subjects ranged in age from 57 to 84 years of age. Individual vertically and horizontally oriented trabeculae were seen within the femoral neck; these correspond to compressive and tensile trabeculae. In addition, the patients demonstrated different degrees of trabecular paucity/deterioration in the femoral neck. For example, there was greater trabecular loss in the 84 year old subject in Figure 4a compared to the 57 year

old in Figure 4c. We also noticed that there was spatial variation in the distribution of trabeculae within the proximal femur, with more prominent trabecular loss within the femoral neck inferiorly compared to other regions.

Finally, we also observed that the superolateral femoral neck cortex was thinner than the inferomedial femoral neck cortex. Finally, we determined whether it would be feasible to image individual trabeculae composing proximal femur microarchitecture when parallel imaging was employed using the 26-element coil setup. Because the trabeculae were poorly seen using the 12-element coil setup without parallel imaging and because of the low 1/g values for the 12-element coil setup, we did not attempt to implement parallel imaging with it because of the further SNR losses. Figures 5a and 5b show representative images from two patients in whom parallel imaging was performed from AF2 through AF4. We also scored the images for ability to depict trabeculae (Figure 5c). Without parallel imaging (AF1), image quality was excellent (4.8±0.4). At AF2, AF3, and AF4, image quality was good (4.3±1.0), average (3.1±1.0), and in the non-visualization range (1.4±0.9), respectively. Differences in image quality between AF1 and AF2 were not statistically significant ($p=0.18$), suggesting AF2 provides an acceptable tradeoff between scan time and image quality. In contrast, differences in image quality between AF2 and AF3 ($p=0.02$) and AF3 and AF4 ($p=0.001$) were statistically significant, indicating compromised image quality.

## Discussion

In this technical note, we have demonstrated the feasibility of using a 26-element receive coil setup to perform 3-D in vivo MRI of proximal femur microarchitecture at 3 T with parallel imaging. We were able to visualize a paucity and spatial variation in the distribution of individual trabeculae within the proximal femur, which is the most devastating site of osteoporotic fracture. With parallel imaging, image quality was good up to AF2. We do note that there was no discernible motion artifact in acquisitions even without parallel imaging (possibly because the pelvis is closer to the axial skeleton and therefore less mobile than the distal extremities, such as the wrist). Nevertheless, the ability to implement parallel imaging and perform faster acquisitions will still reduce the risk of motion artifact.

The 26-element coil provided marked gains in both baseline SNR and parallel imaging performance. Analogous to previous demonstrations of many-element receive arrays in the knee and brain, the improved SNR performance of the 26-element array can be partially attributed to the reduced dimension of its coils, while improved parallel imaging performance can be attributed to the increased number of coil elements (with non-overlapping coil sensitivity profiles) [13,17]. Additionally, the Skyra platform is expected to provide higher baseline performance over the Trio platform by utilizing preamplifiers with lower noise figures and by integrating receive hardware into the magnet housing rather than in an external space. In this study, we used the 26-element coil setup for the application of proximal femur bone microarchitecture imaging; however, the higher SNR and improved parallel imaging performance could also be beneficial for high-resolution cartilage imaging, which is also time-consuming, or even clinical hip imaging, which employs lower-resolution fast spin-echo sequences.

The higher SNR images obtained with the 26-element coil setup allowed depiction of individual trabeculae within the proximal femur, including horizontally and vertically oriented trabeculae, corresponding to tensile and compressive trabeculae, which are critical microstructural components that provide mechanical competence to the proximal femur [18]. The MR images also revealed spatial variation in the distribution of trabeculae as well as varying degrees of trabecular deterioration within the femoral neck. This has been similarly described in prior cadaveric studies of proximal femur specimens scanned by microcomputed tomography [19]. The MR images also reveal thinner cortex along the superolateral femoral neck compared to the inferomedial femoral neck. Mayhew et al. described a similar result in an ex vivo cadaveric specimen study published in the Lancet in 2005 [20]. They concluded that this thinned superolateral femoral neck cortex contributes to patients' hip fracture risk with aging. Beyond our demonstration that this MRI method provides a means to detect microarchitectural deterioration in the femoral neck, we also note that this MRI method might some day provide a means to longitudinally monitor disease progression or the effects of therapy on proximal femur microarchitecture and strength. There is currently no other way to obtain this information in vivo in the proximal femur. Bone biopsy, which is the gold standard for microarchitectural assessment, is limited to the iliac crest and cannot be justified in the femoral neck in osteoporotic subjects.

There are limitations to this study. First, at the voxel size of the images (0.234 mm × 0.234 mm × 1.5 mm, voxel size = 0.082 $mm^3$), we cannot depict trabeculae smaller than 0.234 mm in-plane. Nevertheless, the resolution is still sufficient to visualize individual trabeculae in the femoral neck, and it remains better than the voxel size of current clinical hip MRI (0.41–0.62 mm × 0.41–0.62 mm × 4 mm, voxel size = 0.69–1.56 $mm^3$). In the future, we aim to improve on this resolution. Second, although the multichannel coils and the 128 channel 3 T MRI scanner used in this study are commercially available, they have not yet been widely disseminated. We believe that over time, more centers will acquire such scanners and coils, allowing this research protocol to be applied to a larger patient cohort. Finally, while the gradient echo images acquired in this study enabled outstanding visualization of the bone microarchitecture, fast large angle spin-echo or steady state free precession sequences may achieve greater SNR per unit time and permit higher spatial resolution or shorter scan times [5,6].

In sum, we demonstrate the feasibility of using a novel 26-element receive coil setup to achieve higher SNR and perform, for the first time, 3-D MRI of proximal femur micaroarchitecture in vivo at 3 T without and with parallel imaging. Until now, there have been few studies of bone microarchitecture of the femoral neck, the most devastating site of osteoporotic fracture, because such studies could only be carried out in the ex vivo setting using microcomputed tomography. In the future, it will be necessary to adapt existing digital image analysis tools (e.g., digital topological analysis, finite element analysis) to images of proximal femur microarchitecture, whose complex nature is manifested by a heterogeneous spatial distribution and orientation of trabeculae. Ultimately, this MRI tool may be used as a new research and clinical tool to assess an individual's proximal femur bone quality and potentially, hip fracture risk.

## Acknowledgments

This work was sponsored by United States National Institutes of Health grant K23-AR059748.

## References

1. Kanis JA. Diagnosis of osteoporosis and assessment of fracture risk. Lancet. 2002; 359(9321):1929–1936. [PubMed: 12057569]
2. Burge R, Dawson-Hughes B, Solomon DH, Wong JB, King A, Tosteson A. Incidence and economic burden of osteoporosis-related fractures in the United States, 2005–2025. J Bone Miner Res. 2007; 22(3):465–475. [PubMed: 17144789]
3. Leibson CL, Tosteson AN, Gabriel SE, Ransom JE, Melton LJ. Mortality, disability, and nursing home use for persons with and without hip fracture: a population-based study. J Am Geriatr Soc. 2002; 50(10):1644–1650. [PubMed: 12366617]
4. Stone KL, Seeley DG, Lui LY, et al. BMD at multiple sites and risk of fracture of multiple types: long-term results from the Study of Osteoporotic Fractures. J Bone Miner Res. 2003; 18(11):1947–1954. [PubMed: 14606506]
5. Majumdar S. Magnetic resonance imaging of trabecular bone structure. Top Magn Reson Imaging. 2002; 13(5):323–334. [PubMed: 12464745]
6. Wehrli FW. Structural and functional assessment of trabecular and cortical bone by micro magnetic resonance imaging. J Magn Reson Imaging. 2007; 25(2):390–409. [PubMed: 17260403]
7. Bushberg, J.; Seibert, J.; Leidholdt, E.; Boone, J. The Essential Physics of Medical Imaging. Philadelphia, PA: Lippicont Williams & Wilkins; 2012.
8. Liu XS, Zhang XH, Rajapakse CS, et al. Accuracy of high-resolution in vivo micro magnetic resonance imaging for measurements of microstructural and mechanical properties of human distal tibial bone. J Bone Miner Res. 2010; 25(9):2039–2050. [PubMed: 20499379]
9. Patsch JM, Burghardt AJ, Yap SP, et al. Increased cortical porosity in type 2 diabetic postmenopausal women with fragility fractures. J Bone Miner Res. 2013; 28(2):313–324. [PubMed: 22991256]
10. Burghardt AJ, Kazakia GJ, Sode M, de Papp AE, Link TM, Majumdar S. A longitudinal HR-pQCT study of alendronate treatment in postmenopausal women with low bone density: Relations among density, cortical and trabecular microarchitecture, biomechanics, and bone turnover. J Bone Miner Res. 2010; 25(12):2282–2295.
11. Krug R, Banerjee S, Han ET, Newitt DC, Link TM, Majumdar S. Feasibility of in vivo structural analysis of high-resolution magnetic resonance images of the proximal femur. Osteoporos Int. 2005; 16(11):1307–1314. [PubMed: 15999292]
12. Wright SM, Wald LL. Theory and application of array coils in MR spectroscopy. NMR Biomed. 1997; 10(8):394–410. [PubMed: 9542737]
13. Wiggins GC, Triantafyllou C, Potthast A, Reykowski A, Nittka M, Wald LL. 32-channel 3 Tesla receive-only phased-array head coil with soccer-ball element geometry. Magn Reson Med. 2006; 56(1):216–223. [PubMed: 16767762]
14. Kellman P, McVeigh ER. Image reconstruction in SNR units: a general method for SNR measurement. Magn Reson Med. 2005; 54(6):1439–1447. [PubMed: 16261576]
15. Roemer PB, Edelstein WA, Hayes CE, Souza SP, Mueller OM. The NMR phased array. Magn Reson Med. 1990; 16(2):192–225. [PubMed: 2266841]
16. Pruessmann KP, Weiger M, Scheidegger MB, Boesiger P. SENSE: sensitivity encoding for fast MRI. Magn Reson Med. 1999; 42(5):952–962. [PubMed: 10542355]
17. Chang G, Wiggins GC, Xia D, et al. Comparison of a 28-channel receive array coil and quadrature volume coil for morphologic imaging and T2 mapping of knee cartilage at 7T. J Magn Reson Imaging. 2012; 35(2):441–448. [PubMed: 22095723]
18. Wolff J. The classic: On the significance of the architecture of the spongy substance for the question of bone growth: a preliminary publication 1869. Clin Orthop Relat Res. 2011; 469(11): 3077–3078. [PubMed: 21866420]

19. Milovanovic P, Djonic D, Marshall RP, et al. Micro-structural basis for particular vulnerability of the superolateral neck trabecular bone in the postmenopausal women with hip fractures. Bone. 2012; 50(1):63–68. [PubMed: 21964412]

20. Mayhew PM, Thomas CD, Clement JG, et al. Relation between age, femoral neck cortical stability, and hip fracture risk. Lancet. 2005; 366(9480):129–135. [PubMed: 16005335]

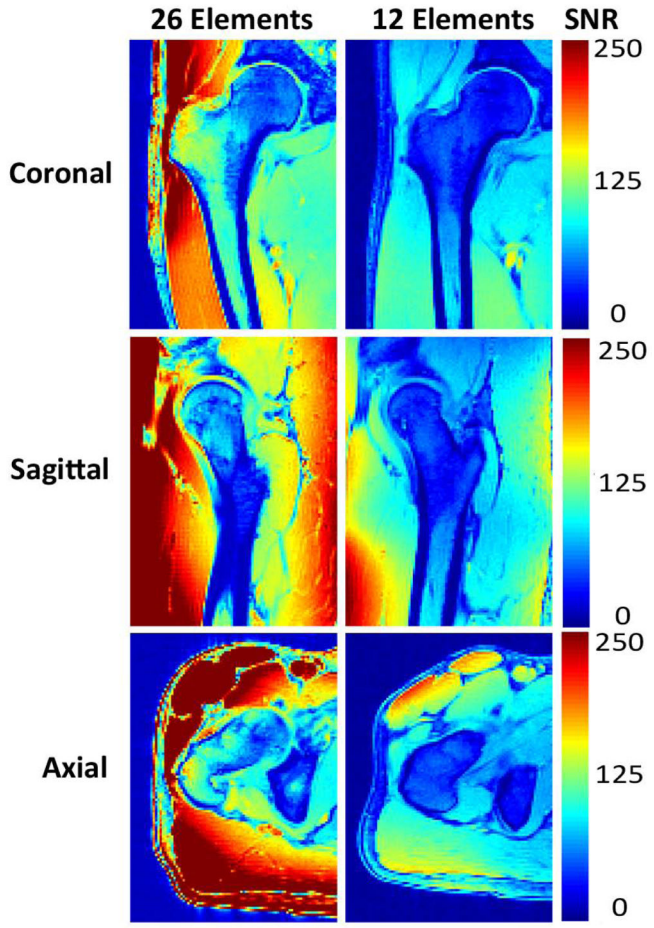


**Figure 1.**

(a) Signal-to-noise ratio (SNR) maps for hip MRI performed with the 26-element coil setup and a 12-element coil setup used for hip MRI. (b) Graphical SNR profile for the coronal hip image. The 26-element coil setup provides higher SNR compared to the 12-element coil setup. The orange dashed line in the image reflects the location where the SNR profiles were obtained.

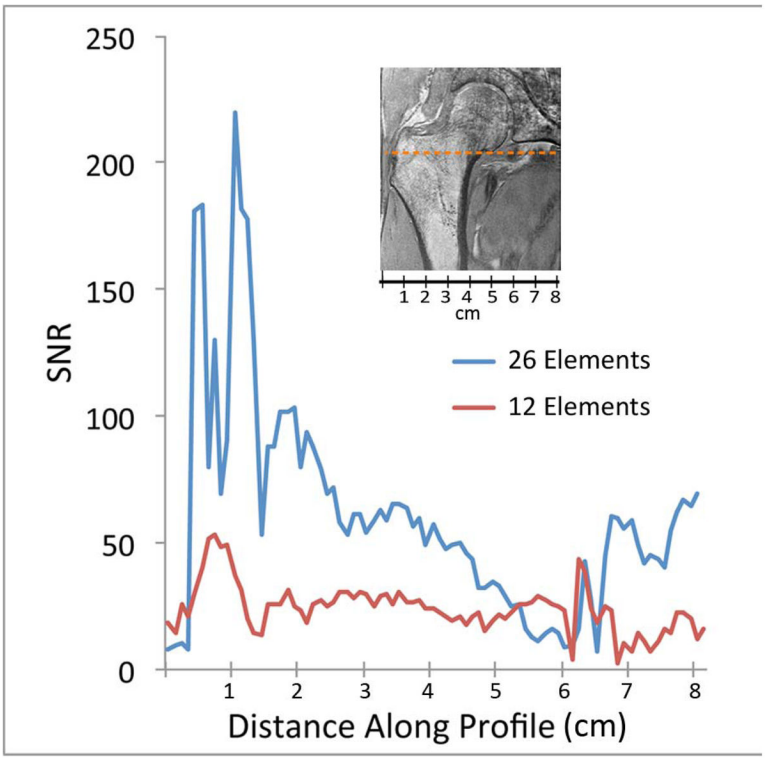


**Figure 2.**

Inverse g-factor maps demonstrate better parallel imaging performance (higher 1/g values at a given acceleration factor) for the 26-element coil setup compared to the 12-element coil setup. The 1/g values listed were measured in the femoral neck (white circle in the corresponding SNR map in left-most panels).

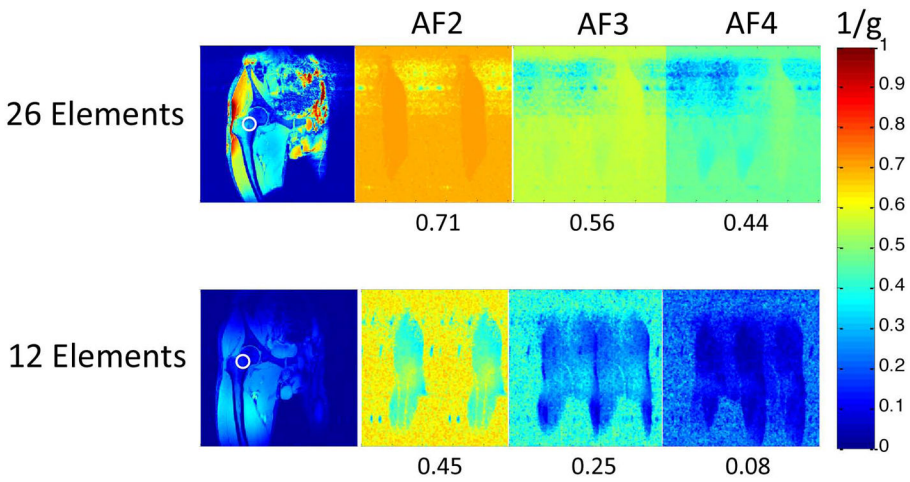


**Figure 3.**

High-resolution coronal images (0.234 mm × 0.234 mm × 1.5 mm) of the left proximal femur in a 68 year old male obtained with the 26-element coil setup and the 12-element coil setup. Individual trabeculae are visible on the image obtained with the 26-element coil setup, but they are poorly seen on the image obtained with the 12-element coil.

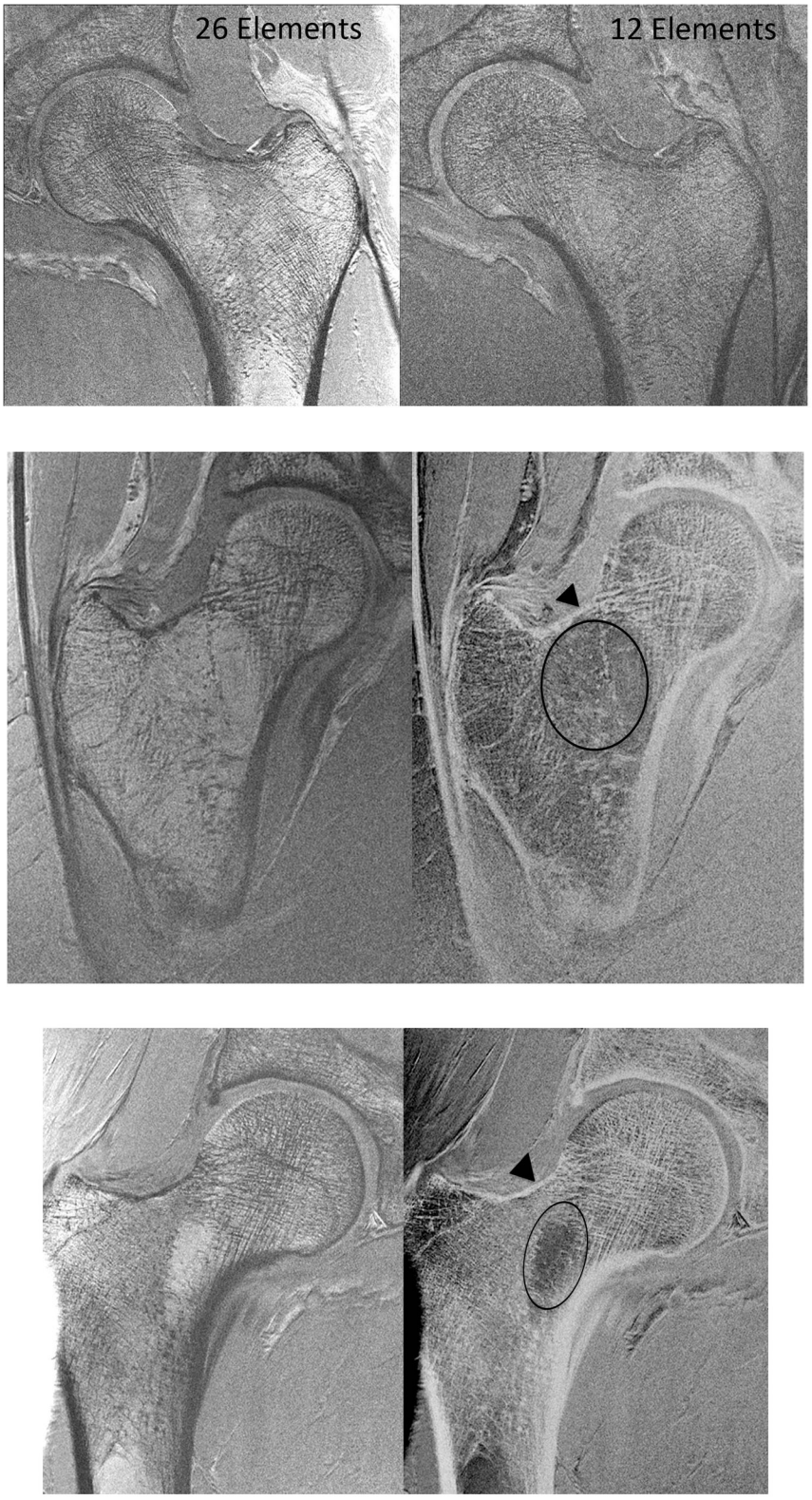

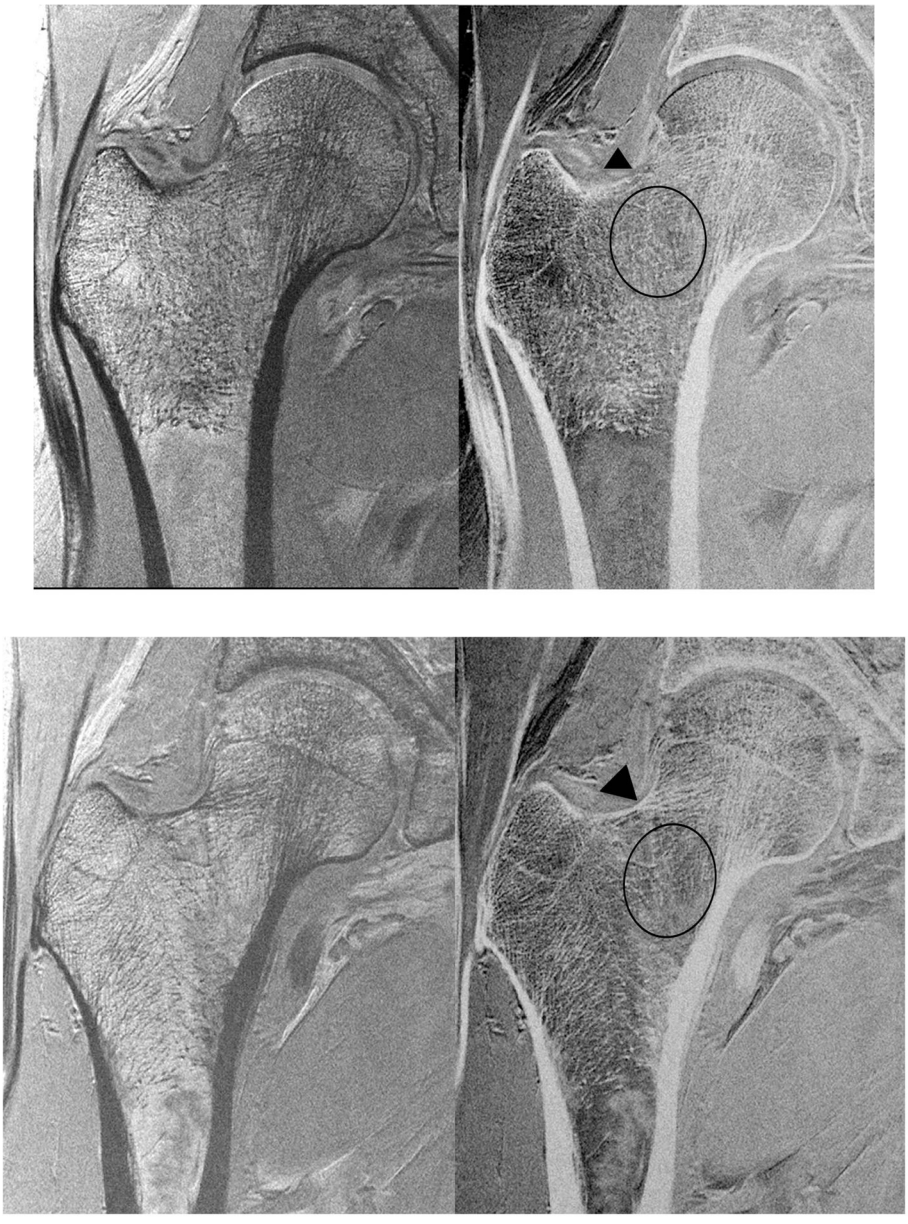

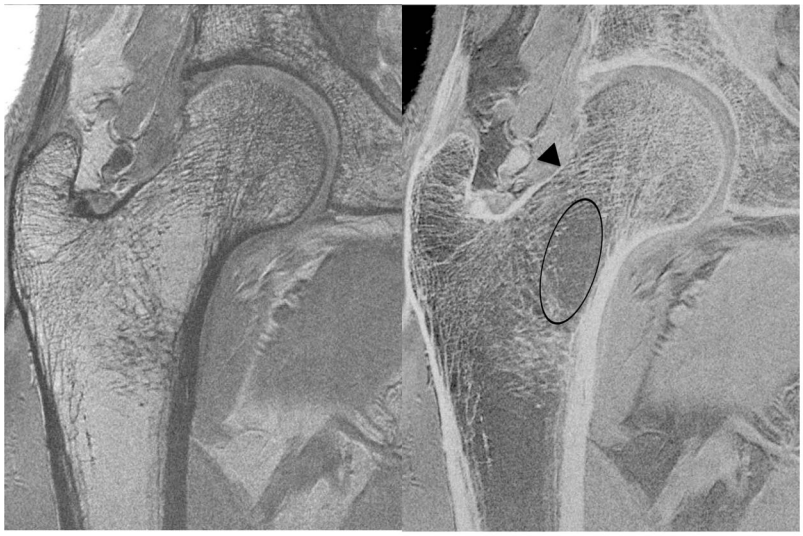

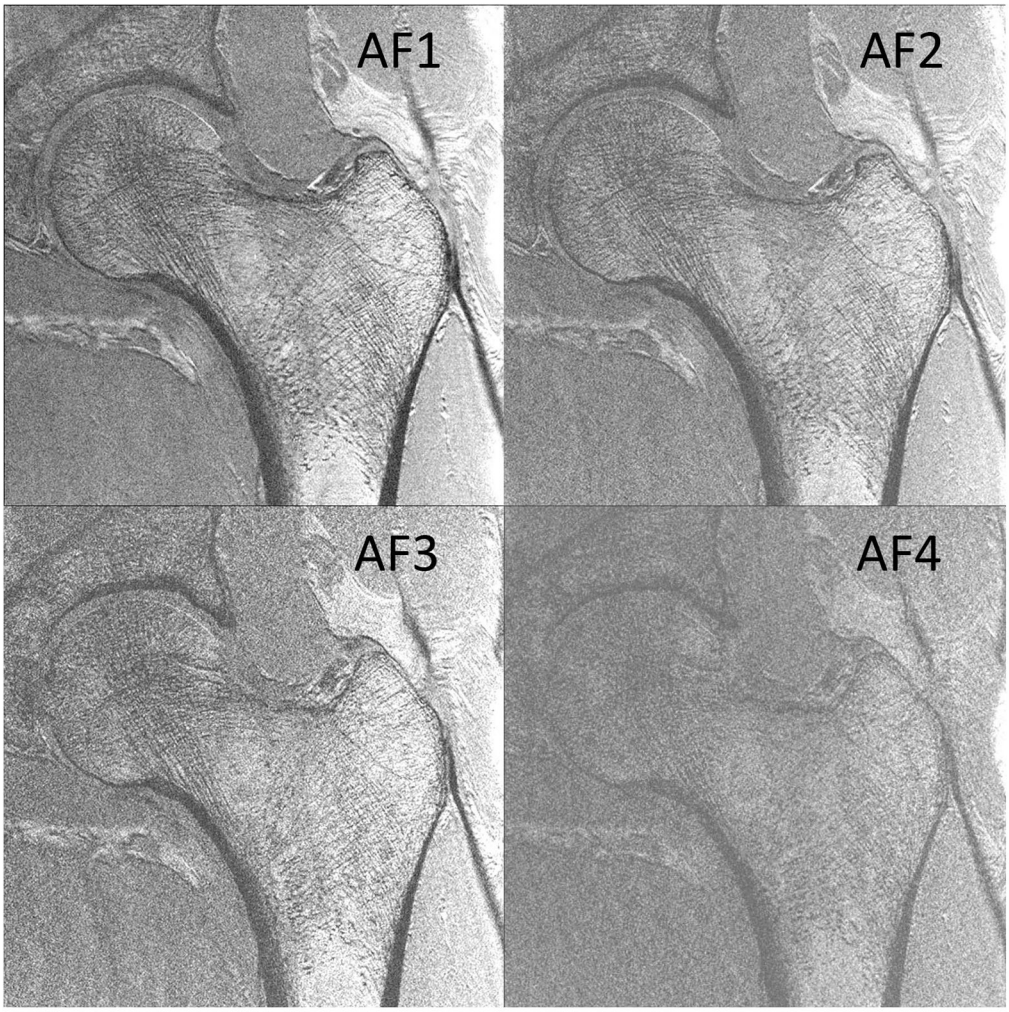

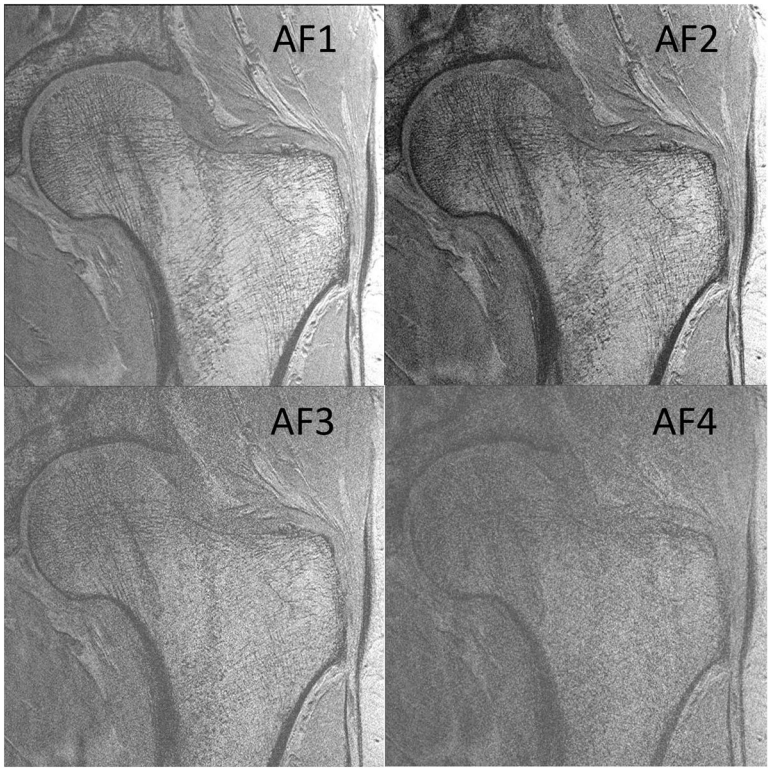


**Figure 4.**

Figure 4a. High-resolution coronal image (0.234 mm × 0.234 mm × 1.5 mm) (left panel) and inverted image (right panel) of the right proximal femur in an 84 year old female obtained with the novel 26-element coil setup. There is paucity of trabeculae across the entire femoral neck (oval), thinning of the superolateral femoral neck cortex compared to the inferomedial cortex (arrowhead), and vertical alignment of compressive trabeculae within the femoral head/neck with the inferomedial femoral neck cortex. More horizontally oriented trabeculae near the femoral head-neck junction correspond to tensile trabeculae.

Figure 4b. High-resolution coronal image (0.234 mm × 0.234 mm × 1.5 mm) (left panel) and inverted image (right panel) of the right proximal femur in a 67 year old male obtained with the novel 26-element coil setup. There is paucity of trabeculae within the inferomedial portion of the femoral neck (oval), superolateral cortical thinning (arrowhead), and vertical alignment of trabeculae within the femoral head/neck with the inferomedial femoral neck cortex.

Figure 4c. High-resolution coronal image (0.234 mm × 0.234 mm × 1.5 mm) (left panel) and inverted image (right panel) of the right proximal femur in 57 year old female obtained with the novel 26-element coil setup. There is paucity of trabeculae in the femoral neck (oval); however, it is not as severe as in the subjects in Figures 4a and 4b. There is superolateral cortical thinning (arrowhead), and vertical alignment of trabeculae within the femoral head/neck with the inferomedial femoral neck cortex.

Figure 4d. High-resolution coronal image (0.234 mm × 0.234 mm × 1.5 mm) (left panel) and inverted image (right panel) of the right proximal femur in a 61 year old female obtained with the novel 26-element coil setup. There is paucity of trabeculae in the femoral neck, more prominent inferomedially (oval). There is superolateral cortical thinning

(arrowhead), and vertical alignment of trabeculae within the femoral head/neck with the inferomedial femoral neck cortex.

Figure 4e. High-resolution coronal image (0.234 mm × 0.234 mm × 1.5 mm) (left panel) and inverted image (right panel) of the right proximal femur in a 67 year old female obtained with the novel 26-element coil setup. There is paucity of trabeculae within the inferomedial femoral neck (oval), superolateral cortical thinning (arrowhead), and vertical alignment of trabeculae within the femoral head/neck with the inferomedial femoral neck cortex.

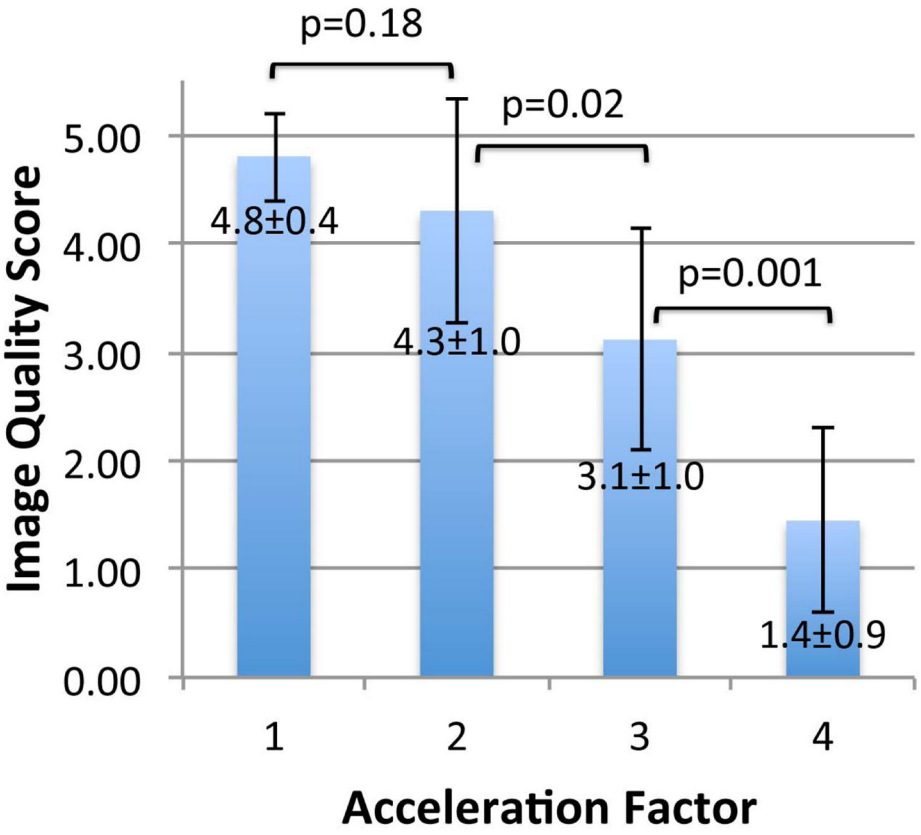


**Figure 5.**

(a) High-resolution coronal image (0.234 mm × 0.234 mm × 1.5 mm) of the left proximal femur in a 68 year old male obtained without parallel imaging (acceleration factor 1 (AF1)) and with parallel imaging at AF2, AF3, and AF4 using the novel 26-element coil setup. (b) High-resolution coronal image (0.234 mm × 0.234 mm × 1.5 mm) images of the left proximal femur obtained in a 65 year old male without parallel imaging (AF1) and with parallel imaging at AF2, AF3, and AF4 using the novel 26-element coil setup. (c) Mean image quality scores (5 = excellent, 4= good, 3 = average, 2 = poor, 1 = non-visualization) at each acceleration factor. Image quality was excellent at AF1, good at AF2, average at AF3, and at the level of non-visualization at AF4. There was no difference in image quality between AF1 and AF2 (p=0.18), but differences in image quality between AF2 and AF3 (p=0.02), and between AF3 and AF4 (p=0.001) were significant.